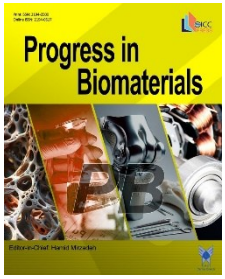

Volume 15, Issue 3, 2025: Article 14

Progress in Biomaterials (PIBM)

https://doi.org/10.57647/pibm.2025.16771

Novel Biocompatible Nanocomposites Based on Gelatin and Green-Synthesized Graphene Quantum Dots for Enhanced Wound Healing

Wessam S. Omara [1], Noha Taymour [2], Sherif H. Kandil [1], Maram A. AlGhamdi[2], Asmaa M. Abd El-Aziz[3,*]

[1] *Department of Materials Science, Institute of Graduate Studies and Research, Alexandria University, Alexandria 21526, Egypt*
[2] *Department of Substitutive Dental Sciences, College of Dentistry, Imam Abdulrahman Bin Faisal University, P.O. Box 1982, Dammam, 31441, Saudi Arabia*
[3] *Fabrication Technology Research Department, Advanced Technology and New Materials Research Institute, City of Scientific Research and Technological Applications (SRTA-City), Alexandria, Egypt*

***Corresponding author:** aabdelaziz@srtacity.sci.eg, chemist_asmaa25@yahoo.com

Original Research

Received:
25 June 2025

Accepted:
03 September 2025

Published in Issue:
30 September 2025

Abstract

Material biology has emerged as a transformative field aimed at addressing biomedical challenges through the development of advanced therapeutic materials that surpass conventional treatment modalities. Biocompatible and highly water-retentive hydrogels have demonstrated significant potential in accelerating diabetic wound healing, mitigating the limitations of traditional wound dressings. This study presents the design and fabrication of a novel gelatin-based hydrogel integrated with graphene quantum dots (GQDs) synthesized via an environmentally sustainable green chemistry approach using natural precursors. The incorporation of GQDs as nanofillers into the gelatin matrix enhanced the physicochemical and biological performance of the resultant nanocomposites hydrogel. FTIR spectra confirmed successful integration of GQDs within the gelatin matrix through characteristic chemical interactions, while XRD analysis demonstrated increased crystallinity reflecting homogeneous GQDs dispersion. Spectroscopic measurements confirmed the exceptional optical properties of GQDs. FESEM images revealed a highly porous morphology with well-distributed GQDs, and TEM analysis verified nanoscale size (~5 nm) and uniform dispersion of GQDs within the hydrogel network. These structural improvements enhanced water uptake and mechanical stability of the hydrogels. Cytotoxicity assessed by MTT assay showed over 90% viability of human skin fibroblast cells, indicating excellent biocompatibility, alongside potent antibacterial activity against *E. coli* assessed by micro-broth dilution. Furthermore, hemocompatibility and thrombogenicity assessments demonstrated the material's safety profile suitable for direct blood contact during wound healing. The findings reveal that the green-synthesized gelatin/GQD nanocomposite hydrogel offers a promising biomaterial scaffold for effective wound management, highlighting its potential to advance therapeutic strategies in diabetic wound healing.

Keywords: Graphene quantum dots; Gelatin hydrogel nanocomposites; Water uptake study; Wound-healing study; Cytotoxicity assay

Cite this article: Omara W.S., Taymour N., Kandil Sh.H., AlGhamdi M.A., Abd El-Aziz A.M., Novel Biocompatible Nanocomposites Based on Gelatin and Green-Synthesized Graphene Quantum Dots for Enhanced Wound Healing. *Progress in Biomaterials,* 15(3), Article 14. https://doi.org/10.57647/pibm.2025.16771

Graphical in Biomaterials

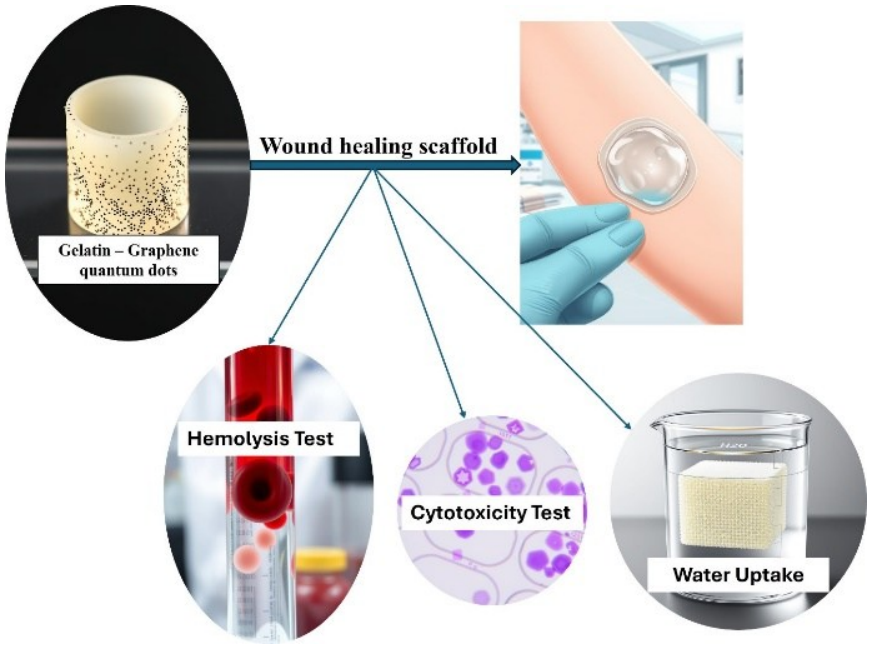

1. Introduction

Wound healing remains a significant clinical challenge worldwide, particularly in complex cases such as diabetic ulcers, where conventional treatments often fail to provide satisfactory outcomes[1]. The development of advanced biomaterials that can actively support and accelerate tissue regeneration has thus become a major focus in regenerative medicine and biomaterials. Hydrogels, with their high water content and extracellular matrix-mimicking properties[2], have emerged as promising wound dressings that maintain a moist environment conducive to tissue repair while acting as carriers for bioactive agents and nanomaterials[3]. Among natural polymers, gelatin, a denatured form of collagen, has attracted considerable attention due to its excellent biocompatibility, biodegradability, low immunogenicity, and cell-friendly characteristics that favor wound healing processes such as cell adhesion and proliferation[4, 5].

Despite the inherent advantages of gelatin-based hydrogels, challenges remain in improving their mechanical stability, antibacterial efficacy, and bioactivity to meet the multifaceted demands of wound repair[6]. The integration of nanomaterials, particularly carbon-based nanostructures, has provided a versatile strategy for enhancing these properties[7][8]. Graphene and its derivatives, including graphene quantum dots (GQDs), have shown exceptional potential due to their unique physicochemical and biological properties[9][10][11].Graphene quantum dots, nanoscale fragments of graphene with distinctive quantum confinement and edge effects[12], exhibit superior photoluminescence, high surface area, and excellent biocompatibility, making them suitable candidates for biomedical applications including wound healing[13][14]. Their ability to facilitate electron transfer catalysis can enhance reactive oxygen species [ROS) scavenging or generation, crucial for modulating inflammation and antimicrobial activity at the wound site[13].

However, the synthesis of graphene quantum dots has conventionally relied on harsh chemical methods involving toxic reagents[15], expensive precursors, and energy-intensive processes[10]. These conventional fabrication routes pose environmental concerns and limit large-scale, cost-effective production, ultimately hindering clinical translation[16][17]. This highlights a critical knowledge gap which is the need for environmentally sustainable and economically feasible synthetic methods that yield biocompatible graphene quantum dots suitable for wound healing applications[18]. Green synthesis approaches have recently emerged as promising alternatives, employing natural precursors such as plant extracts, biomass waste, or simple carbohydrates, combined with facile hydrothermal, microwave, or pyrolytic treatments to produce GQDs under mild, eco-friendly conditions[19].

These methods minimize toxic byproducts and enhance the biological safety of the resulting nanomaterials, yet their integration into wound dressing development remains underexplored.

In this context, our study addresses this gap by developing a novel biocompatible nanocomposite hydrogel based on gelatin incorporated with green-synthesized graphene quantum dots. We employ a sustainable green synthesis route using natural precursors to fabricate GQDs, thereby advancing eco-friendly nanotechnology integration into wound care. The resulting gelatin/GQD hybrid hydrogel is designed to leverage the inherent water-retaining and cell-supportive properties of gelatin, augmented by the electron transport capabilities, photoluminescence, and antibacterial activity of GQDs to promote enhanced wound healing efficacy.

This work contributes to the field of biomaterials by demonstrating an innovative, facile, and environmentally responsible synthesis of graphene quantum dots and their effective incorporation into gelatin hydrogels. We comprehensively characterize the physicochemical interactions, morphology, cytocompatibility, hemocompatibility, and antibacterial properties of the nanocomposite, with an emphasis on its application as advanced wound dressing. The synergy between biopolymer and carbonaceous nanomaterial under green synthesis paradigms offers significant advancement in the design of smart, bioactive wound care systems addressing both material performance and sustainability demands.

2. Materials and Methods

2.1. Materials

The materials used in this study are listed in Table 1.

2.2. Preparation of graphene Quantum dots (GQDs)

Graphene Quantum dots were prepared according to the thermal pyrolysis method (TPM) of organic materials as a carbon source, in which minor modifications were introduced to obtain GQDs by green methods[20]. TPM is likely a new green method for synthesizing GQDs that uses citric acid as a carbon source. White fine crystals of lemon salt (2 g) were placed in a 5 mL beaker and melted in a mineral oil bath (Glycerol) at 290 o C for 30 minutes; the color started to change to pale yellow and finally became orange. The melted orange solution was reduced by its addition dropwise within 15 minutes into Ammonium hydroxide solution (15%, 100 mL) under vigorous stirring. Finally, a clear yellow solution of GQDs was obtained, as shown in Scheme 1.

2.3. Preparation of gelatin/graphene quantum dots nanocomposites

A gelatin solution (5 Wt.%) was prepared by dissolving in distilled water (DW). However, in the case of Gelatin / GQDs, composites were made by dissolving gelatin (5 Wt. %) in the resulting GQDs solution (result from 2.2 step). The prepared gelatin composites were with (5 and 10) % of GQDs with the codes [G-5GQDs, G-10GQDs]. All solutions were dissolved for 2 hours at 40 °C as shown in Scheme (2). The hydrogels were subsequently cross-linked using 5 µL. mL^{-1} glutaraldehyde (GTA) and stirred at room temperature for one hour. The cross-linked samples were thoroughly rinsed with deionized water to eliminate any residual from GTA. Before characterization, the resulting nanocomposite hydrogels were cooled to -20°C overnight and then lyophilized in a freeze dryer for 48 hours to achieve interconnected porous structures.

2.4. Characterization of the prepared GQDs and gelatin hydrogel nanocomposites

Surface morphology and structural details of the freeze-dried [G, and G/GQDs "it indicates for the high concentration of GQDs into gelatin, (G/10GQDs)"] nanocomposites were analyzed by different techniques, which are shown on Table 1. Dynamic light scattering and zeta potential are measured on liquid samples of GQD concentrations between 8 mg/mL. Utilizing Tauc's method (eq. 1) to determine the absorption coefficient (α) of this concentration and the refractive index (RI) was calculated via eq. 2[21][22]

$$\alpha = \frac{2.303 \times A}{l\,(cm)} \quad (1)$$

$$RI = \frac{1}{T_s} + \sqrt{\frac{1}{T_s - 1}} \quad (2)$$

Where A is the absorbance of the GQD solution at 633 nm, and Ts is the transmittance calculated 10-A x 100. L is the path length of the sample utilized in the microplate reader which was 0.294 cm (100 µL of GQD solution in 96 well-plate). The α at 8 mg/mL is 2.3367 and RI at 0.1623. These parameters were implemented in the Malvern nano-ZS90 (Worcestershire, UK) software and the zeta potential and size were determined accordingly.

2.5 Water Uptake

Weighed samples of lyophilized hydrogels were immersed in water at 37 ℃ for a specified period. After immersion, samples were removed, gently blotted with filter paper, and reweighed. The swelling test was conducted in triplicate for each sample (n=3), and the swelling percentage of each hydrogel was determined using Equation 3.

$$Swelling\ \% = [(w_s - w_d)/w_d] \times 100 \quad (3)$$

Where wd is the weight of the hydrogel after soaking at a definite time interval and drying the gel, while ws is the weight of the swollen hydrogel at a definite time.

2.6 Biocompatibility assessment

A biocompatibility assessment including hemocompatibility, thrombogenicity, and cytotoxicity, are carried out to examine the suitability of materials in biomedical applications[23].

2.6.1 *Hemocompatibility test*

Following the American Society for Testing and Materials guidelines (ASTM F 756-00, 2000), the hemolysis test was conducted as proposed.[24] Firstly, 9 mL of rabbit blood (Ethical Approval # AU 14 -231120-1-5) was gently added to a tube containing 1 mL of anticoagulant (ACD).

Each lyophilized hydrogel sample (0.05 g) was then immersed in a test tube with 7 mL of phosphate buffer solution (PBS) at pH 7.0 and maintained at 37°C for 72 hours before being exposed to the rabbit blood. Following the removal of the phosphate buffer solution (PBS), the samples were incubated in 1 mL of ACD-treated blood at 37°C for 3 hours.

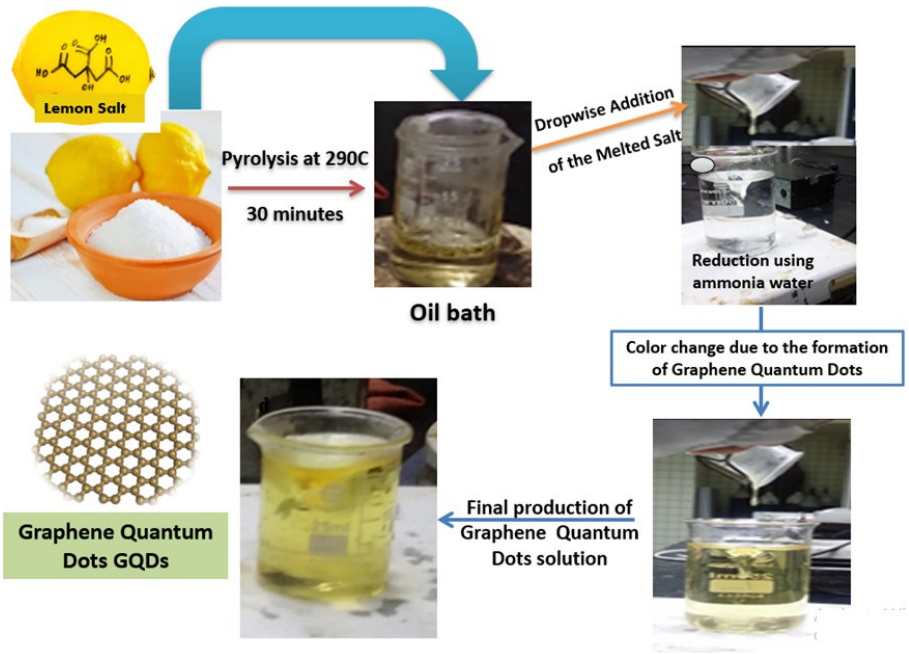

Scheme 1. The Green synthesis of GQDs

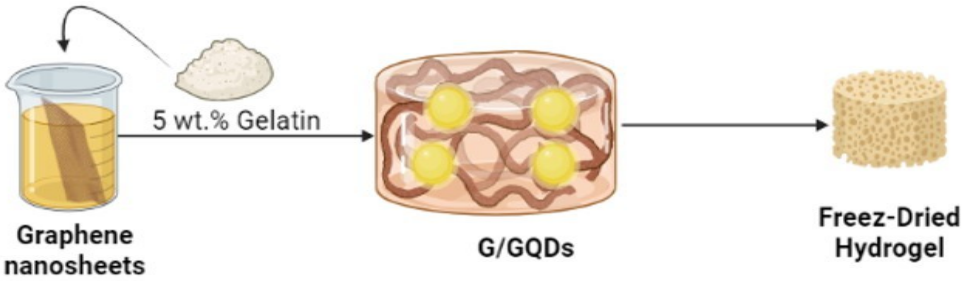

Scheme 2. Preparation of the Gelatin / GQDs hydrogel nanocomposite

Table 1. Materials used for this study

Material	Source
Lemon Salt (food grade)	Local render
Ammonia hydroxide (NH_4OH)	Sigma-Aldrich
Gelatin from bovine skin (Type B)	Sigma-Aldrich Chemical Co., St. Louis, MO, USA
Acid citrate dextrose solution (ACD)	Sigma-Aldrich (Chemie GmbH, Steinheim, Germany)
RPMI 1640	Corning, NY, USA
Trypsin	Corning, NY, USA
Trypan blue	Corning, NY, USA
Penicillin-streptomycin	Corning, NY, USA
L-glutamine	Corning, NY, USA
Phosphate buffer saline tablets	GeneTex, Irvine, CA, USA
Fetal bovine serum	Lonza, Switzerland
MTT	Serva, Heidelberg, Germany
Dimethyl sulfoxide	Carbo-Elba, Milan, Italy
Formaldehyde Solution	Sigma-Aldrich

Table 2. Armamentarium used in gelatin/GQDs hydrogel nanocomposites characterization

Device/Equipment	Manufacturer	Purpose/ Application
Scanning Electron Microscope (SEM) (JEOL JSM 6360LA)	JEOL, Japan	Examine the structure and morphology of GQDs and freeze-dried gelatin/GQD hydrogel composites.
Transmission Electron Microscope (HR-TEM) (JEOL 2100 PLUS)	JEOL, Japan	Imaging, revealing crystal structures, conducting elemental analysis (qualitative and semi-quantitative), and diffraction pattern imaging.
Eagle CCD Camera (4k x 4k resolution)	JEOL, Japan	Capture and record transmitted electron images during TEM analysis.
Fourier Transform Infrared Spectrometer (FTIR)	Perkin-Elmer, USA	Study the chemical structures of GQDs and gelatin/GQDs composites over a wavenumber range of 4000-400 cm^{-1}.
X-ray diffractometer (XRD) (Shimadzu X-ray 7000)	Shimadzu, Japan	Perform X-ray diffraction scans to assess the crystallinity of prepared hydrogels using a copper target source.
UV-Vis spectrophotometer	Evolution 600 double beam scanning UV-visible spectrophotometer, Thermo scientific, USA	Measure the absorbance of GQDs in the range of 200-900 nm
Fluorescence spectroscopy	a PerkinElmer LS-55 spectrofluorometer at 650-900 V.	This instrument uses a pulsed xenon source to minimize the photobleaching of GQDs and provides a long-lived excitation source. The variable slit and holographic gratings provide flexibility with very low stray radiation.
Spectrophotometer (λ = 540 nm)	Not specified	Measure haemoglobin released due to hemolysis during blood hemolysis tests.
Centrifuge (2000 rpm)	Not specified	Clarify blood and samples during hemolysis testing.
Microplate Reader (Fluorostar Omega)	BMG labtech	Measure the absorbance at 570 nm for MTT cytotoxicity assays and at 600 nm for antibacterial studies.
Incubator (37°C)	Local vendor	Maintain hydrogel samples and cells at physiological temperature during swelling tests, biocompatibility, and cytotoxicity studies.
Water Bath	Not specified	Halt the thrombus formation reaction during the thrombogenicity test.
Lyophilizer	Taisite- China	Freeze-dry hydrogel samples for water uptake and characterization studies.

To create negative and positive controls, equal volumes of ACD blood were mixed with 7 mL of PBS and water, respectively. To avoid direct contact between the test materials and blood, the tubes were gently inverted twice every 30 minutes.

Finally, both the blood and diluted samples were transferred to new tubes and clarified by centrifugation at 2000 rpm for 15 minutes. A spectrophotometer calibrated to λ = 540 nm was employed to quantify the hemoglobin released as a result of hemolysis. Blood hemolysis experiments were conducted in triplicate under the same conditions, and the hemolysis percentage was determined by using Equation [4].

$$Blood\ hemolysis\ \% = \left[\frac{ODs-ODn}{ODp-ODn}\right] \times 100 \qquad (4)$$

Where ODs is the optical density of a tested sample, ODn refers to the optical density of the negative control, and ODp is the optical density of the positive control.

2.6.2 *Thrombogenicity test.*

A gravimetric method was employed to evaluate thrombus formation on the surface of the developed hydrogel, as previously suggested. Initially, the lyophilized hydrogels were immersed in phosphate buffer solution (PBS) and incubated at 37 °C for 48 hours. After this period, PBS was removed, and ACD-treated rabbit blood was applied to the surface of the samples under investigation, with an equal blood volume placed in an empty Petri dish to serve as a positive control. To initiate the blood clotting reaction, calcium chloride (20 µL, 10 M) solution was added on top of each sample. After 45 minutes, the reaction was halted by adding 5 mL of water. The formed clots were subsequently fixed with 5 mL of formaldehyde solution, and dried using tissue paper, before weighing. Each test was conducted in triplicate. [25]

2.6.3 *Cytotoxicity assay*

Cells preparation

The human skin fibroblast cell line was cultured in RPMI 1640 basal medium, supplemented with 10% FBS, 1% L-glutamine, and 1% penicillin-streptomycin. Cells were then harvested from T-flasks using trypsinization with 0.25% trypsin-EDTA for 1 minute and then collected by centrifugation at 500 x g (relative centrifugal force) for 5 minutes. The supernatant was removed, the pellet was resuspended in the growth medium, and the cells were counted using the trypan blue exclusion assay.

MTT assay

The cells were seeded at a density of (10*104 cells/well) in a 96-well plate and allowed to attach overnight. To create a concentration gradient ranging from (100% to 6.25%), the samples (GQDs, G/10GQDs, G/5GQDs, and Gelatin) were first diluted with growth medium to a concentration of 10%, which is the maximum allowed concentration according to ISO 10993-5. The first five columns of the plate were then filled with decreasing dilutions of the GQDs to achieve concentrations of (100%, 50%, 25%, 12.5%, and 6.25%) for each sample. After incubating the cells with the samples for 24 hours, (20 µL of 5 mg/mL) MTT was added to each well and incubated for an additional 3 hours. The media was then replaced with DMSO to dissolve the formazan dye, and the absorbance was measured at ʎ= 570 nm using a Fluorostar Omega plate reader.

$$Viability\ (\%) = \frac{Abs.of\ test\ material}{Abs.of\ negative\ control} \times 100 \qquad (5)$$

2.7. Antibacterial Activity

Micro-broth dilution method / MIC Test: “according to CLSI M07-A10” was used. Three bacterial strains were used in this study, Pseudomonas aeruginosa (27853), Escherichia coli (ATCC 25922), and Staphylococcus aureus (ATCC 6538). The bacterial strains were cultured overnight in nutrient broth and set at a cellular concentration of 1 x 108 cells / mL by OD of 0.1 at 600 nm. The concentrations of GQD used were 50, 25, 12.5, 6.25, and 3.125 mg/mL (n=3). 50 µL of GQD solution was aspirated in a 96-well plate with 50 µL of bacterial strain giving a final cellular density of 5x106 cells/well. The well plate was incubated at 37°C for 24 hours and then analyzed with a microplate reader set to 600 nm.

$$Viability\ (\%) = \frac{Abs.of\ test\ material}{Abs.of\ negative\ control} \times 100 \qquad (6)$$

2.8. Statistical analysis:

Data is expressed as mean ± standard deviation (SD). Statistical Significance differences between test groups were tested using one-way analysis of variance (ANOVA) and Bonferroni post-hoc test performed using PSPP software (version 1.6.2). P-values <0.05 were considered statistically significant. Weibull method was used for the cytotoxicity and antibacterial activity.

3. Results and Discussion

3.1 Characterization of G/GQDs hydrogel nanocomposites

The chemical composition and structure of graphene

quantum dots (GQDs), and G/GQDs gelatin nanocomposite were investigated using FTIR, XRD, and Optical analysis of GQDs as shown in Figure 1. The FTIR spectrum of GQDs includes the peaks at 1620 cm-1 and 1470 cm-1 which correspond to the skeletal vibrations of the GQD aromatic rings[26]. A band at 1552 cm^{-1} is associated with C=C stretching vibrations. Additionally, FTIR signals observed around 3400, 1654, and 1400 cm^{-1} are indicative of O–H stretching, C=O stretching of carboxyl groups, and aromatic C=C stretching, respectively[27–29]. The gelatin has characteristic peaks at 1659 cm-1 which indicate the occurrence of amide-I, while the peak at 1554 cm-1 indicates amide-II, and the weak band at 1240 cm-1 shows the amide-III band, which is allocated to the triple-helix of collagen[30].

In the spectra of the G/GQD hydrogel nanocomposite, several peaks confirm successful carboxamide functionalization. These include a weak amide III peak at 1396 cm^{-1}, a C=C aromatic peak at 1451 cm^{-1}, a medium amide II peak at 1544 cm^{-1}, a peak of C=O at 1654 cm^{-1}, medium C-H stretching vibrations of methyl and methylene groups near 2926 cm^{-1}, and strong stretching vibrations of O-H and N-H around 3434 cm^{-1} [31].

X-ray diffraction (XRD) patterns are used to study the crystallinity of GQDs. The XRD patterns of GQDs in Figure (1B, 1C), which show a broad peak at around (2θ=24°) correspond to the 002 crystal plane [35,36]. The XRD pattern of the GQDs shows a broad (002) peak, indicating an interlayer spacing of 0.37 nm, which is greater than that of graphite (0.33 nm). This increase in spacing may be attributed to the disordered stacking of certain GQDs[37]. Gelatin hydrogel has also a broad diffraction peak at 2θ=23° and may be the crosslinking and freeze-drying in the process of hydrogel composite preparation depress the crystallization of the gelatin and results in an almost indiscernible flat and broad diffraction peak. [38].

The electronic absorption spectra of GQDs were measured using UV-Vis spectrophotometer (Evolution 600 double beam scanning UV-visible spectrophotometer, Thermo scientific, USA) in the range of 200-900 nm. The sample was prepared in a clear and diluted liquid form. The UV absorption spectrum Figure (1D) shows a peak of GQDs located at 220 nm due to the Π-Π* transition from the aromatic sp2 domain of GQDs with a long tail extending into the visible range due to the n-Π* transition. However, another shoulder absorption peak could be observed in the wavelength region from 290 to 360 nm (n-Π*) due to –C= O. The peak position is more sensitive to the preparation method than the size of the dots and also depends on the medium used for measurement[32][33]. Characteristic fluorescence properties of GQDs were revealed as shown by the apparent absorption below 400 nm[34].

The photoluminescence PL and fluorescence emission of GQDs were detected by exciting the GQDs sample at 300 nm and measuring the resulting emission peak centered at 453 nm as shown in Figure (1E, 1F). The excitation-dependent PL is a characteristic of GQDs and could also be related to the presence of the defect and different functional groups on GQDs[35].

The band gap of GQDs was measured as shown in Figure (1F), It means that an electron must absorb at least 2.73 eV of energy (≈ 454 nm photon, blue region of visible light) to jump from the valence band to the conduction band and become electrically conductive.

The GQD was tested for approximate particle size and homogeneity via the DLS. By calculation of DLS, a particle size of 254 nm with a PDI of 0.427 at a concentration of 4mg/mL. This is considered a good estimation of our particle size to be smaller than 250 nm due to the hydration shell surrounding the GQD, giving an overestimated particle size. The actual particle size is readily determined via TEM. On the other hand, GQD's ZP was also measured at the same concentration having a surface charge of -28.3 mV and 2.5 mS/cm as conductivity. This negative surface charge would predict that the developed GQD will have an antibacterial activity, as studied before in previous literature [19][39]. Hence, the GQD developed is a good candidate to bind to bacteria and hinder their activity.

Field emission scanning electron microscopy (FE-SEM) data of GQDs revealed that rather than the expected individual GQDs, nano aggregates were formed with a size range of (10 to 100) nm as shown in Figure (2A). All hydrogel samples were lyophilized after being freeze-dried at -80 °C in liquid nitrogen. Figure (2B, 2C) shows the SEM micrographs of freeze-dried gelatin hydrogel G. All of the hydrogels had well-connected porous architectures, with typical pore diameters of about (216 ± 69) μm (measured by image J). But in case of G/GQDs, the SEM images Figure (2D, 2 E) show the pores were compacted and pore size decreased, this may be due to the electrostatic interactions between the GQDs and positively charged groups within gelatin[6].

The TEM image of the resulting GQDs, with diameters ranged from (3.77 to 7.37) nm, which confirms that GQDs are in the quantum range, where their size is less than 10 nm as it is shown in Figure (3A). High-resolution TEM images and the corresponding fast Fourier transform (FFT) pattern of the GQD show a high crystalline structure with a lattice parameter of about 0.24 nm.[40]. TEM images of G/GQDs hydrogel nanocomposite, Figure (3B) show high dispersion of the GQDs particles in the gelatin hydrogel.

3.2 Water uptake of the gelatin hydrogel composites

The swelling ratio of the prepared G/GQDs hydrogels reflects their ability to absorb wound exudates produced during the inflammatory phase of healing. To assess this, the hydrogels were incubated in a phosphate buffer solution (PBS) at 37 °C for various time intervals before being weighed. As depicted in Figure 4, the G/GQDs sample exhibited a considerably higher swelling ratio compared to the unmodified gelatin control. The water-uptake ratios were very high, reaching 700 % in the case of the modified sample due to the hydrophilicity enhancement of GQDs inside the gelatin hydrogel. This enhanced performance can be also attributed to the greater porosity and specific surface area of GQDs in comparison to pure gelatin.

The pore size of gelatin hydrogel unmodified was approximately 100-150 µm that is very comparable to the modified G/GQDs hydrogel. But this difference on swelling ability may be the hydrophilicity enhancement of GQDs that are due to functional groups O-H, C=O, that attract water molecules and increase water uptake ability.

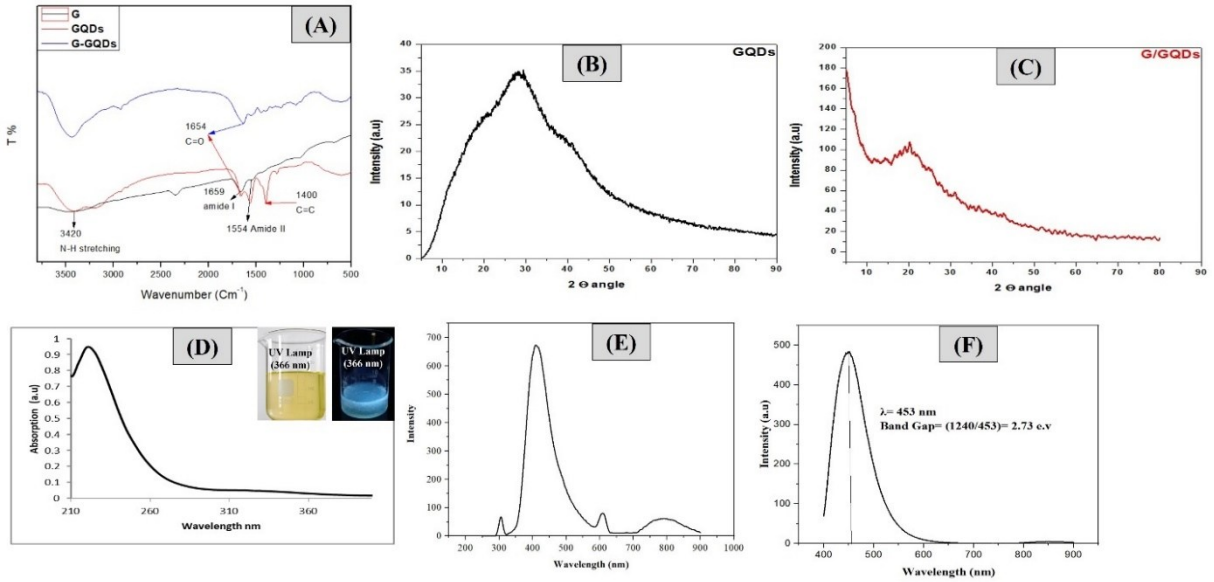

Figure 1. Physical characterization of the prepared GQDs and G/10GQDs hydrogel nanocomposite (A): FTIR, (B,C): XRD analysis of GQDs, and G/GQDs respectively, (D): Absorption spectrum of GQDs, with the photo of the GQDs in daylight and under the UV lamp. (E, F): photoluminescence and Fluorescence spectrum of GQDs

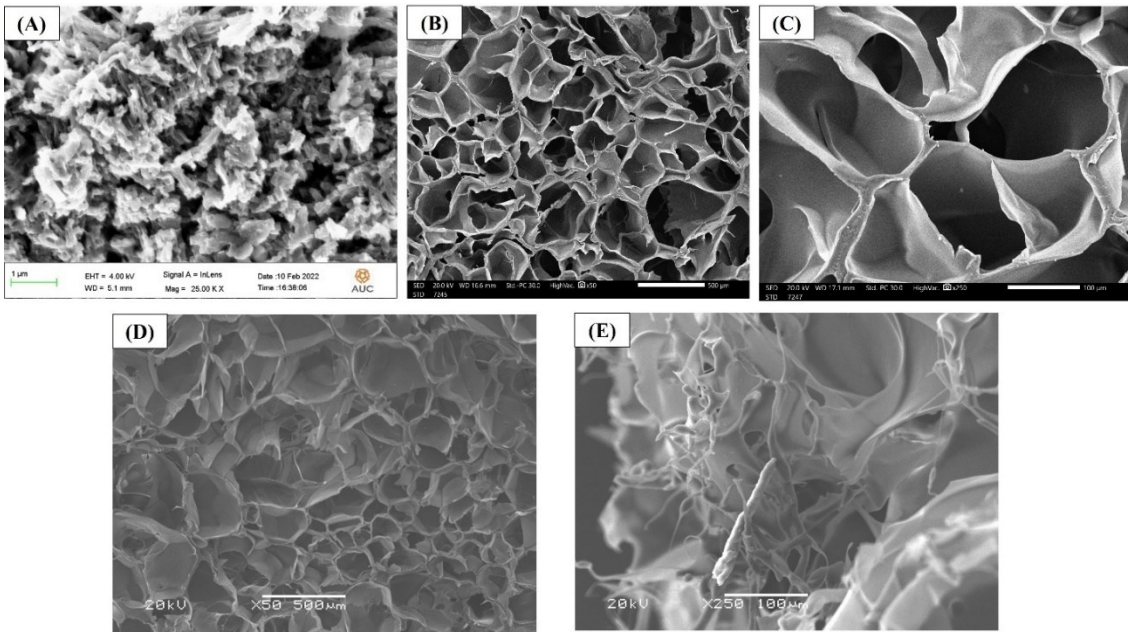

Figure 2. Morphological analysis of the synthesized GQDs and G/GQDs hydrogel nanocomposites (A): SEM image of GQDs, (B, C): SEM images of G hydrogel at 50X, and 250 X magnifications respectively, (D, E): SEM images of G/GQDs at 50X, and 250 X magnifications respectively

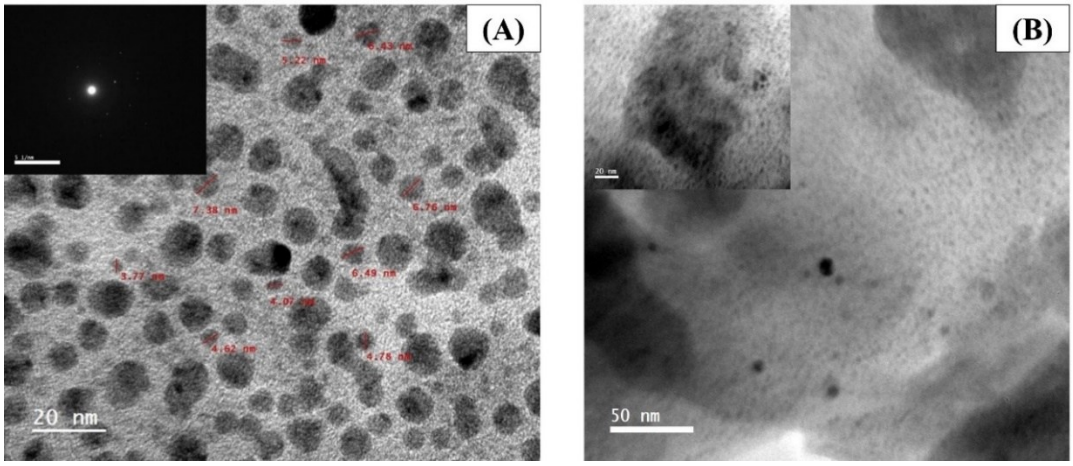

Figure 3. TEM images of (A): GQDs with high resolution crystal structure on the Upper-left side, (B): G/GQDs hydrogel nanocomposite with high magnification on the upper-left image at 20 nm

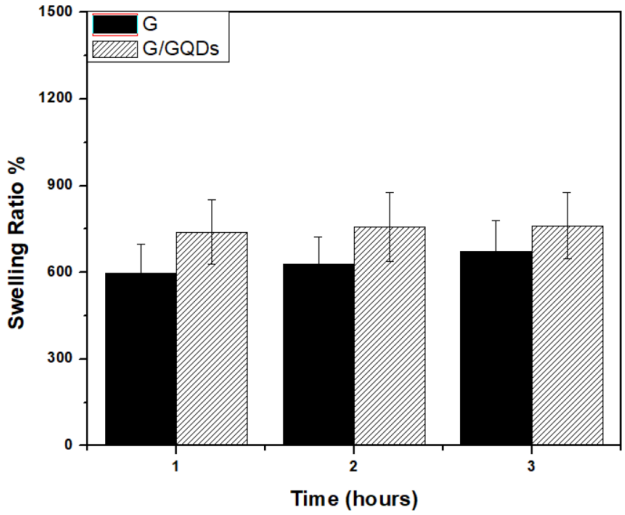

Figure 4. Swelling study of GQDs, and G/GQDs hydrogel composite

3.3 Biocompatibility evaluation

3.3.1 *Hemocompatibility and Thrombogenicity*

Evaluating blood compatibility is crucial for biomaterials that come into direct or indirect contact with blood. The hemolysis test provides an essential in-vitro preliminary screening to assess blood compatibility. Figure (5A) illustrates the hemolytic percentages of the G and G/GQDs samples examined. The results indicated a modest increase in hemolytic activity between the control and G/GQDs nanocomposites. Nevertheless, the hemolysis percentage for all prepared samples remained below 2%, which is deemed safe according to ASTM F 756-00, 2000. These results come in alignment with earlier studies. [13,41] The prepared samples were determined to be compatible with materials that do not cause hemolysis. hrombogenicity is a critical characteristic of materials used in wound healing. Figure (5B) demonstrates that gelatin exhibited a lower propensity for thrombus formation compared to the positive control and G/GQDs. This difference may be linked to the intrinsic ability of GQDs to promote integrin-mediated platelet activation and adhesion.[13] Consequently, the G/GQDs hydrogel proved to be an excellent biodressing material, effectively maintaining moisture in the wound during the healing process. GQDs significantly enhance the healing mechanism due to their exceptional electron transport properties, which facilitates high peroxidase-like activity. Hydrogen peroxide (H_2O_2) is commonly employed for wound disinfection to prevent bacterial infections; however, high concentrations of H_2O_2 can be detrimental to healthy tissue and may impede the healing process. Hence, it is essential to improve the antibacterial effectiveness of H_2O_2 while reducing the concentration required for effective germicidal action in wound disinfection.

3.3.2 *Cytotoxicity analysis*

The prepared G/GQDs hydrogels have been tested for

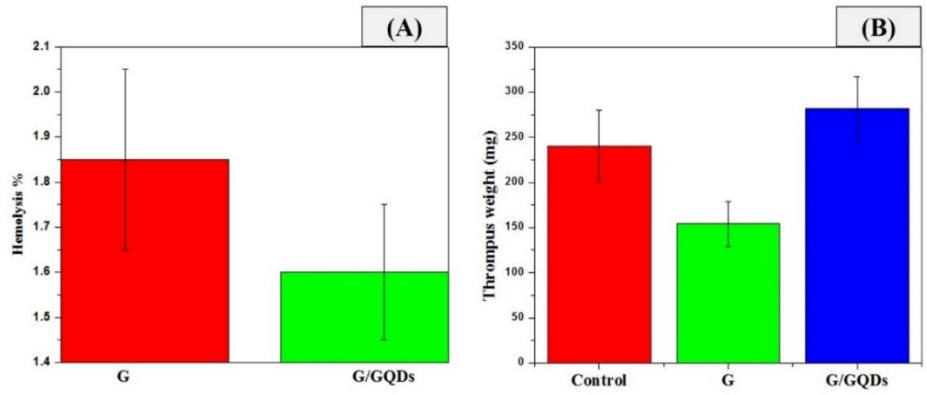

Figure 5. (A) Haemocompatibility, (B) Thrombogenicity for GQDs, and G/GQDs hydrogel composite

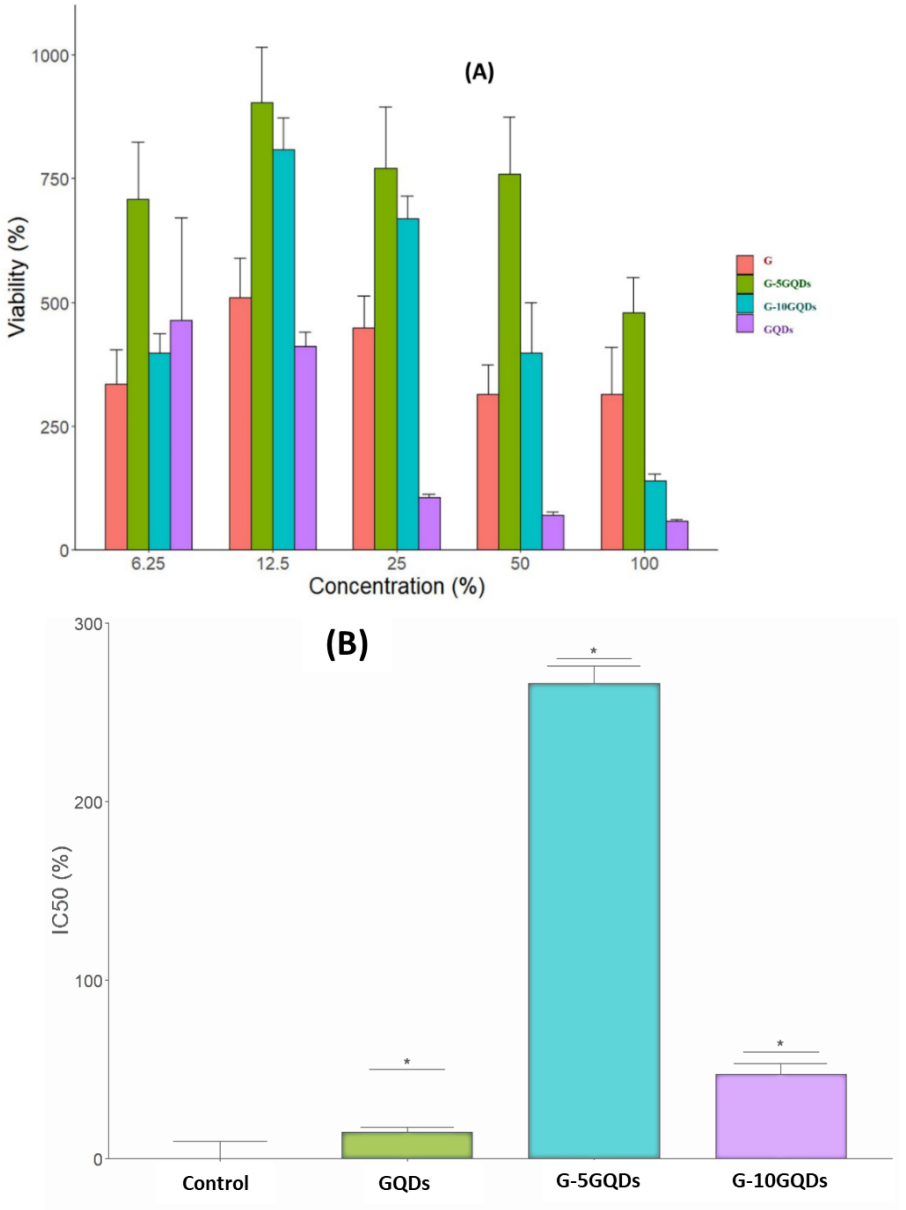

Figure 6. MTT assay of Human Skin fibroblast cells. The results shown are normalized with the absorbance of a normal growth medium. A) Shows the viability of the cells at increasing concentrations of GQDs. B) Shows the IC50 of the GQDs based on the Weibull method; * p-value <0.0001. The error bars are standard error

10.57647/pibm.2025.16771

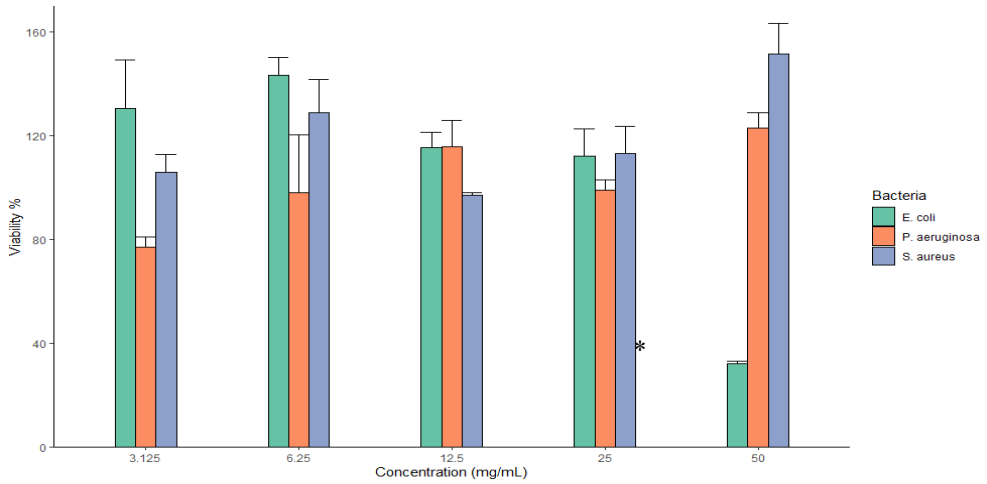

Figure 7. Viability of the three bacterial strains showing their viability against the concentration of GQDs

cytotoxicity against human fibroblast skin cells (HFS).They are first diluted (10% v/v) in a growth medium to allow the cells to proliferate with nutrients, growth factors and minerals found in the medium. Therefore, control is employed and ensured, according to Figure (6), that the dilution step and the gradient concentrations (6.25-100%) didn't affect the growth of the cells. The cells grew rapidly, given the vehicle that dissolves gelatin which promotes cell growth. [42], [43] However, as shown in Figure (6A) the viability of the HFS cells decreased as the gradient concentration of GQDs increased. At 25-100% of the pure GQD, the HFS cells viability was 105%, 70.25%, and 57.8% respectively. While at 6.25-12.5% of the pure GQD, the cell's viability was comparable to the control gelatin (464%, and 410%) respectively. G/5GQDs showed better cellular viability in contrast with G/10GQDs.

The inhibitory concentration 50 (IC50) is a pharmacodynamics parametric sigmoid scale showing how toxic or non-toxic a given medical device or vehicle. There are several parametric IC50 scales the one used in this study is Weibull scale due to its use in toxicity. Figure(6B) shows the summary of the IC50 of the samples with their error bar as standard error and the p-values are denoted in an asterix. The highest toxicity is the pure GQD with an IC50 of 14.7%, in contrast with G/5GQDs was not considered toxic at all owing to its expected toxicity at a larger concentration at 265%. However, G/10GQDs' IC50 was at a concentration of 47.4% gradient concentration. Therefore, with the respective results GQD is considered toxic to cells from (1-10) %, but G/5GQDs solution is considered safe.

3.3.3 *Antibacterial Activity*

GQD showed an enhanced viability towards bacteria even at the highest concentrations except E. coli. At 50 mg/mL of GQD, E. coli suffered a significant viability of 32.2% against its control compared with P. aeruginosa (122.9%), and S. aureus (151.1%), Figure (7). At 12.5 mg/mL of GQD, there is a significant difference between the viability of S. aureus (97%) and E. coli (115.5%). Finally, at 3.125 mg/mL of GQD, P. aeruginosa showed a lower viability (77%) against E. coli (130%) and S. aureus (106%). E. coli showed an IC50 of 22.4 mg/mL with a standard error of 5.7 mg/mL, but at lower concentrations, E. coli showed enhanced viability. Whereas the other two strains didn't show a definitive IC50 suggesting that the concentration of IC50 is higher than the concentration range used in this study. This result is due to the negative charge of GQDs, which repelled from the negatively charged sites on bacterial membranes (S. aureus, P. aeruginosa, E. coli). But in case of, E. coli it was more susceptible towards GQD (viability <50% at 50 mg/mL of GQD) than P. aeruginosa, and S. aureus[44][45].

4. Conclusion

Dressings made with biocompatible films hold promise for wound care due to their ability to maintain a conducive environment, form a physical barrier, and prevent bacterial infiltration, all of which help sustain a balanced healing ecosystem. By dissolving gelatin in a solution containing graphene quantum dots (G/5, 10 GQDs) hydrogel nanocomposite. In addition to supplying good moisture and accelerating epithelization, the newly developed composite hydrogels demonstrated good wound fluid absorption and water retention.

The prepared samples were determined to be compatible with materials that do not cause hemolysis. The developed nanosystem addresses the limitations of isolated treatments and the standalone use of antibiotics

in clinical settings by integrating the distinctive properties of nanomaterials, photodynamic effects, and pharmaceuticals. All of these experiments and their evaluated findings suggest that newly created G/GQDs nanocomposite hydrogels have a significant potential for use as dressings for wounds, both as disinfectants and for dressings in wound healing. In the recommendation for this work that increase functionalization of GQDs and also study its photodynamic activity on both different bacterial and cellular membranes.

Funding

There is No Fund support.

Ethical Approval:

The test of Hemocompatibility has been approved by the Committee of Ethics at the Institute of Graduate Studies and Research, Alexandria University, Egypt, under the number (AU 14 -231120-1-5).

Acknowledgment

We acknowledge Saif El-Din Al-Mofty, a researcher at the Department of Chemistry, School of Sciences & Engineering, The American University in Cairo, New Cairo, Egypt. He assisted us with the antibacterial testing.

Authors Contribution

All authors have contributed equally to prepare the paper.

Availability of data and materials

The data that support the findings of this study are available from the corresponding author, upon reasonable request.

Conflict of interests

The authors declare that they have no known competing financial interests or personal relationships that could have appeared to influence the work reported in this paper.

References

[1] Ribeiro ERFR, Correa LB, Ricci-Junior E, Souza PFN, dos Santos CC, de Menezes AS, et al. Chitosan-graphene quantum dot based active film as smart wound dressing. J Drug Deliv Sci Technol. 2023;80(December 2022).

[2] El-Nablaway M, Rashed F, Taher ES, Foda T, Abdeen A, Abdo M, et al. Prospectives and challenges of nano-tailored biomaterials-assisted biological molecules delivery for tissue engineering purposes. Life Sci. 2024;349(February).

[3] El-Nablaway M, Rashed F, Taher ES, Atia GA, Foda T, Mohammed NA, et al. Bioactive injectable mucoadhesive thermosensitive natural polymeric hydrogels for oral bone and periodontal regeneration. Front Bioeng Biotechnol. 2024;12(May):1–31.

[4] Zhang Y, Wang J. Current status and prospects of gelatin and its derivatives in oncological applications: Review. Int J Biol Macromol. 2024;274(P1):133590.

[5] Serag E, Eltawila AM, Salem EM, El-Maghraby A, Abd El-Aziz AM. Development of an innovative cylindrical carbon nanofiber/gelatin-polycaprolactone hydrogel scaffold for enhanced bone regeneration. Int J Biol Macromol. 2025 May;306(Pt 2):141250.

[6] Wang N, Xu H, Sun S, Guo P, Wang Y, Qian C, et al. Wound therapy via a photo-responsively antibacterial nano-graphene quantum dots conjugate. J Photochem Photobiol B Biol. 2020;210(February):111978.

[7] Nasser Atia GA, Mohamed SZ, Taymour N, Soliman MM, Halim HA, Shalaby HK, et al. Carbon Dots as Promising Carbon Nanomaterials for Diagnostics, Therapeutics, and Regenerative Orofacial Applications. J Drug Deliv Sci Technol. 2025;106808.

[8] Taymour N, Haque MA, Atia GAN, Mohamed SZ, Rokaya D, Bajunaid SM, et al. Nanodiamond: A Promising Carbon-Based Nanomaterial for Therapeutic and Regenerative Dental Applications. Vol. 9, ChemistrySelect. 2024.

[9] Khoshkalampour A, Ghorbani M, Ghasempour Z. Cross-linked gelatin film enriched with green carbon quantum dots for bioactive food packaging. Food Chem. 2023;404(PB):134742.

[10] Ni F, Chen Y, Wang Z, Zhang X, Gao F, Shao Z, et al. Graphene derivative based hydrogels in biomedical applications. J Tissue Eng. 2024;15.

[11] Yu CH, Chen GY, Xia MY, Xie Y, Chi YQ, He ZY, et al. Understanding the sheet size-antibacterial activity relationship of graphene oxide and the nano-bio interaction-based physical mechanisms. Colloids Surfaces B Biointerfaces. 2020;191(March):111009.

[12] Sadek KM, Shib NA, Taher ES, Rashed F, Shukry M, Atia GA, et al. Harnessing the power of bee venom for therapeutic and regenerative medical applications: an updated review. Front Pharmacol. 2024;15(July).

[13] Sun H, Gao N, Dong K, Ren J, Qu X. Graphene quantum dots-band-aids used for wound disinfection. ACS Nano. 2014;8(6):6202–10.

[14] Martins VGFC, Alencar LMR, Souza PFN, Lorentino CMA, Frota HF, dos Santos ALS, et al. Wound dressing using graphene quantum dots: a proof of concept. J Pharm Investig. 2023;53(2):333–42.

[15] Wang S, Cole IS, Li Q. The toxicity of graphene quantum dots. Vol. 6, RSC Advances. 2016.

[16] Gozali Balkanloo P, Mohammad Sharifi K, Poursattar Marjani A. Graphene quantum dots: synthesis, characterization, and application in wastewater treatment: a review. Vol. 4, Materials Advances. 2023.

[17] Tian P, Tang L, Teng KS, Lau SP. Graphene quantum dots: preparations, properties, functionalizations and applications. Mater Futur. 2024;3(2).

[18] Zhong X, Tong C, Liu T, Li L, Liu X, Yang Y, et al. Silver nanoparticles coated by green graphene quantum dots for accelerating the healing of: MRSA-infected wounds. Biomater Sci. 2020;8(23).

[19] Kadyan P, Thillai Arasu P, Kataria SK. Graphene Quantum Dots: Green Synthesis, Characterization, and Antioxidant and Antimicrobial Potential. Int J Biomater. 2024;2024.

[20] Zor E, Morales-Narváez E, Zamora-Gálvez A, Bingol H, Ersoz M, Merkoçi A. Graphene quantum dots-based photoluminescent sensor: A multifunctional composite for pesticide detection. ACS Appl Mater Interfaces. 2015;7(36):20272–9.

[21] Ditta MA, Farrukh MA, Ali S, Younas N. X-ray peak profiling, optical parameters and catalytic properties of pure and CdS doped ZnO–NiO nanocomposites. Russ J Appl Chem. 2017;90(1).

[22] Yasmeen S, Iqbal F, Munawar T, Nawaz MA, Asghar M, Hussain A. Synthesis, structural and optical analysis of surfactant assisted ZnO–NiO nanocomposites prepared by homogeneous precipitation method. Ceram Int. 2019;45(14).

[23] Yang KR, Hong MH. Improved Biocompatibility and Osseointegration of Nanostructured Calcium-Incorporated Titanium Implant Surface Treatment (XPEED®). Materials (Basel). 2024;17(11).

[24] Alves P, Santos M, Mendes S, Miguel SP, de Sá KD, Cabral CSD, et al. Photocrosslinkable nanofibrous asymmetric membrane designed for wound dressing. Polymers (Basel). 2019;11(4):1–18.

[25] Serag E, Abd AM, Aziz E, Maghraby A El, Taha NA. Electrospun non - wovens potential wound dressing material based on polyacrylonitrile / chicken feathers keratin nanofiber. Sci Rep. 2022;1–14.

[26] Gontrani L, Pulci O, Pizzoferrato R. Detection of heavy metals in water using graphene quantum dots : an experimental and theoretical study. 2021;(July):1–14.

[27] Wazir A, Kundi IW, Bannu T. Synthesis of graphene nano sheets by the rapid reduction of electrochemically exfoliated graphene oxide induced by microwaves Synthesis of Graphene Nano Sheets by the Rapid Reduction of Electrochemically Exfoliated Graphene Oxide Induced by Microwaves. 2016;(February).

[28] Janowska I, Chizari K, Ersen O, Zafeiratos S. Electronic Supplementary Material Microwave Synthesis of Large Few-Layer Graphene Sheets in Aqueous Solution of Ammonia. 2010;(February).

[29] Jeong S, Pinals RL, Dharmadhikari B, Song H, Kalluri A, Debnath D, et al. Graphene Quantum Dot Oxidation Governs Noncovalent Biopolymer Adsorption. Sci Rep. 2020;10(1):1–14.

[30] Cao S, Wang Y, Xing L, Zhang W, Zhou G. Structure and physical properties of gelatin from bovine bone collagen influenced by acid pretreatment and pepsin. Food Bioprod Process. 2020;121:213–23.

[31] Javanbakht S, Nabi M, Shaabani A. Graphene quantum dots-crosslinked gelatin via the efficient Ugi four-component reaction: Safe photoluminescent implantable carriers for the pH-responsive delivery of doxorubicin. Materialia. 2021;20(July):101233.

[32] Kundu S. Synthesis and characterization ofgraphene quantum dots. Phys Sci Rev. 2019;1–35.

[33] Zarghami A, Dolatyari M, Mirtagioglu H, Rostami A. High-efficiency upconversion process in cobalt and neodymium doped graphene QDs for biomedical applications. Sci Rep. 2023;13(1):1–14.

[34] Diao J, Wang T, Li L. Graphene quantum dots as nanoprobes for fluorescent detection of propofol in emulsions. R Soc Open Sci. 2019;6(1).

[35] Gebreegziabher GG, Asemahegne AS, Ayele DW, Mani D, Narzary R, Sahu PP, et al. Polyaniline–graphene quantum dots (PANI–GQDs) hybrid for plastic solar cell. Carbon Lett. 2020;30(1):1–11.

[36] Tian P, Tang L, Teng KS, Lau SP. Graphene quantum dots from chemistry to applications. Mater Today Chem. 2018;10:221–58.

[37] Krishnamoorthy K, Veerapandian M, Kim G shik, Jae S. A One Step Hydrothermal Approach for the Improved Synthesis of Graphene Nanosheets A One Step Hydrothermal Approach for the Improved Synthesis of Graphene Nanosheets. 2012;(December).

[38] Yazdimamaghani M, Vashaee D, Assefa S, Walker KJ, Madihally S V., Köhler GA, et al. Hybrid macroporous gelatin/bioactive-glass/nanosilver scaffolds with controlled degradation behavior and antimicrobial activity for bone tissue engineering. J Biomed Nanotechnol. 2014;10(6):911–31.

[39] Bing W, Sun H, Yan Z, Ren J, Qu X. Programmed Bacteria Death Induced by Carbon Dots with Different Surface Charge. Small. 2016;12(34).

[40] Liu F, Jang MH, Ha HD, Kim JH, Cho YH, Seo TS. Facile synthetic method for pristine graphene quantum dots and graphene oxide quantum dots: Origin of blue and green luminescence. Adv Mater. 2013;25(27):3657–62.

[41] Joshi P, Ahmed MSU, Vig K, Vega Erramuspe IB, Auad ML. Synthesis and characterization of chemically crosslinked gelatin and chitosan to produce hydrogels for biomedical applications. Polym Adv Technol. 2021;32(5):2229–39.

[42] Saotome T, Shimada N, Matsuno K, Nakamura K, Tabata Y. Gelatin hydrogel nonwoven fabrics of a cell culture scaffold to formulate 3-dimensional cell constructs. Regen Ther. 2021;18:418–29.

[43] Łabowska MB, Cierluk K, Jankowska AM, Kulbacka J, Detyna J, Michalak I. A review on the adaption of alginate-gelatin hydrogels for 3D cultures and bioprinting. Materials (Basel). 2021;14(4):1–28.

[44] Lado-touriño I, Alicia P. Interaction between Graphene-Based Materials and Small Ag , Cu , and CuO Clusters : A Molecular Dynamics Study. Nanomaterials. 2021;11(1378):15.

[45] Dizaj SM, Mennati A, Jafari S, Khezri K, Adibkia K. Antimicrobial activity of carbon-based nanoparticles. Adv Pharm Bull. 2015;5(1).